PCCP

PAPER

View Article Online
View Journal | View Issue

Cite this: *Phys. Chem. Chem. Phys.*, 2018, **20**, 1476

Angstrom-scale probing of paramagnetic centers location in nanodiamonds by ^{3}He NMR at low temperatures†

Vyacheslav Kuzmin, *[a] Kajum Safiullin, *[a] Gleb Dolgorukov, [a] Andrey Stanislavovas, [a] Egor Alakshin, [a] Timur Safin, [a] Boris Yavkin, [a] Sergei Orlinskii, [a] Airat Kiiamov, [a] Mikhail Presnyakov,[b] Alexander Klochkov [a] and Murat Tagirov [ac]

Received 29th August 2017,
Accepted 5th December 2017

DOI: 10.1039/c7cp05898e

rsc.li/pccp

In this article a method to assess the location of paramagnetic centers in nanodiamonds was proposed. The nuclear magnetic relaxation of adsorbed ^{3}He used as a probe in this method was studied at temperatures of 1.5–4.2 K and magnetic fields of 100–600 mT. A strong influence of the paramagnetic centers of the sample on the ^{3}He nuclear spin relaxation time T_1 was found. Preplating the nanodiamond surface with adsorbed nitrogen layers allowed us to vary the distance from ^{3}He nuclei to paramagnetic centers in a controlled way and to determine their location using a simple model. The observed T_1 minima in temperature dependences are well described within the frame of the suggested model and consistent with the concentration of paramagnetic centers determined by electron paramagnetic resonance. The average distance found from the paramagnetic centers to the nanodiamond surface (0.5 ± 0.1 nm) confirms the well-known statement that paramagnetic centers in this type of nanodiamond are located in the carbon shell. The proposed method can be applied to detailed studies of nano-materials at low temperatures.

Introduction

Nanodiamonds are a subject of many recent scientific studies because of their broad spectrum of potential applications, including abrasives or catalysts, biosensors and electrodes.[1,2] Nanodiamonds are composed of a crystal core and shell of amorphous layers. The shell of unpurified nanodiamonds can be covered by various functional groups or chemical compositions depending on the application and method of nanodiamond preparation.[1] Nowadays the most popular methods to prepare nanodiamond powders are HPHT (high pressure high temperature), CVD (chemical vapor deposition), DND (detonation technique) and milling methods.[1] Different types of paramagnetic centers can exist in a diamagnetic matrix of nanodiamonds:[1] radical-type centers in the shell, radical-type centers on the surface, various implemented paramagnetic impurities on the surface, NV centers in the nanodiamond core, *etc.* It is known that purified detonation nanodiamonds contain paramagnetic centers only in the nanodiamond shell.[1] The amount and type of paramagnetic center determine the application of nanodiamonds and their commercial value. Usually cw and pulse electron paramagnetic (EPR), electron nuclear double (ENDOR), nuclear magnetic (NMR) and optically detected magnetic (ODMR) resonance methods are used to determine the properties of paramagnetic centers and their possible locations in nanodiamonds.[3–7]

The application of NV centers as nanoscale sensors of the surrounding environment is an actively developing field of research. Shallow NV centers have recently been applied as atomic-sized NMR sensors[8] that allow the performance of nanoscale NMR with 1 ppm resolution.[9] Experimental realization of the predefined near-surface deposition of NV centers could be done using, *e.g.* the δ-doping technique which allows one to form arrays of NV centers with exceptional spin coherence properties.[10,11] The experimental technique that allows one to determine the actual depth of the NV center deposition inside the nanoparticle is in high demand.

^{3}He is a premium candidate for studies of the magnetic properties of nanosized samples at low temperatures due to the absence of a nuclear quadrupole moment and sufficiently long intrinsic T_1 relaxation times. Therefore ^{3}He nuclear magnetic relaxation can be sensitive to the magnetism of the sample. Properties of adsorbed ^{3}He are well understood and it is

[a] *Institute of Physics, Kazan Federal University, 420008 Kazan, Russian Federation. E-mail: slava625@yandex.ru, kajum@inbox.ru; Fax: +7 843 233 7355; Tel: +7 843 233 7306*
[b] *National Research Centre "Kurchatov Institute", 123182 Moscow, Russian Federation*
[c] *Academy of Sciences of the Republic of Tatarstan, Institute of Perspective Research, 420111 Kazan, Russian Federation*

† Electronic supplementary information (ESI) available. See DOI: 10.1039/c7cp05898e

commonly used as a model system of 2D solids with quantum exchange at low temperatures.[12–14] Usually it is assumed that nuclear magnetic relaxation in this system occurs due to dipole–dipole interactions modulated by quantum exchange or thermal 2D motions.[14,15] There are also many studies of direct dipole–dipole interactions between adsorbed ^{3}He and nuclear[16,17] spins or indirect interactions with electronic spins inside the solids.[18,19] Similar direct dipolar couplings were also observed in liquid ^{3}He surrounding solid samples.[20,21]

In this article we present a new technique that provides detailed information on the magnetic properties of the surface layer of solids and the distribution of paramagnetic impurities in nanodiamonds. It is based on the measurement of relaxation times of adsorbed ^{3}He distant from the sample surface by variable adsorbed layer thickness of noble or inactive gases. The observed minima in T_1 temperature dependences provide direct information on correlation times and local magnetic fields.[12,22,23] The proposed method allows the variation of the distance between the ^{3}He layer and paramagnetic centers and allows one to obtain information on its distribution in nanoparticles.

Experimental

Detonation nanodiamond powder of 98.3% purity produced by US Research Nanomaterials, Inc. (USA) was used as a sample. The declared by manufacturer particle size of the powder is 3–10 nm and the average particle density $\rho \approx 3.18$ g cm^{-3}. The powder was rammed down while placed into a 6 mm i.d. experimental Pyrex cell sealed to the ^{3}He gas managing system *via* the capillary. The 180 mg sample is 12 mm in length which corresponds to a sample porosity of 83%. Before every experiment the experimental cell was flushed several times with helium-4 at 95 °C temperature and then pumped out.

Pulsed ^{3}He NMR experiments were performed at 1.5–4.2 K temperatures and in the range of resonance frequencies f_0 = 5–19 MHz using a laboratory made NMR spectrometer[24] with a glass cryostat. The purity of ^{3}He used in the NMR experiments was better than 99.99%. The ^{3}He spin–lattice relaxation time T_1 was measured by a saturation-recovery technique. The ^{3}He nuclei transverse magnetization relaxation time T_2 was obtained by a standard Hahn echo sequence.

Some experiments were performed with the sample surface covered by a certain amount of solid N_2 layers. The presence of nitrogen nuclei (^{14}N I = 1) with a quadrupole moment does not have an influence on ^{3}He nuclei magnetization relaxation as the corresponding cross-relaxation process is expected at lower NMR frequencies ($\approx$3.48 MHz).[25] Careful annealing of nitrogen layers was done in order to prevent any effects of nonuniformity of the N_2 layers. For this purpose the sample was connected to a large volume balloon where a necessary amount of N_2 gas was introduced at room temperature and then the sample temperature was slowly lowered down to 4.2 K. In order to achieve homogenous nitrogen distribution on the sample surface and create proper nitrogen layers we fulfilled the following conditions during nitrogen adsorption. During a slow temperature decrease the nitrogen gas pressure was carefully managed to be significantly below saturated vapor pressure values[26] that excluded capillary condensation. According to estimates these measures prevent any undesirable effects of capillary condensation in the pores of nanodiamond powder larger than a few nanometers in diameter.

Sample characterization

XRD measurements

The nanodiamond powder properties were studied by X-ray diffraction experiments on a Bruker D8 Advance diffractometer at Kazan Federal University. The obtained X-ray diffraction pattern is presented in Fig. 1. Three main peaks (111), (220) and (311) of the pattern are attributed to the crystal structure of the nanodiamond core. The pattern shows the absence of a graphite phase in the sample: there is no visible corresponding broad line near $2\theta = 25^\circ$.[27,28] The low-intensity broad line near $2\theta = 63^\circ$ is known to represent the amorphous a-C phase of sp^2-carbon.[29] This verifies that nanodiamond particles are composed of diamond cores and of amorphous carbon layers on the top of the core.[1]

Implementation of the Scherrer equation for a spherical shape of nanodiamonds allows us to estimate the average diamond core diameter d_{core}: $d_{core} = 0.9\lambda/(\beta \cos\theta)$, where the X-ray wavelength λ = 0.154 nm and β is the FWHM of the peak at θ. The d_{core} estimates made for three pattern peaks give almost the same values with the average $d_{core} = 4.24 \pm 0.06$ nm.

TEM measurements

Transmission electron microscopy (TEM) was performed on a Titan 80-300 S/TEM (FEI, USA) at the Probe and Electron microscopy RC ''NANOPROBE'', National Research Center ''Kurchatov Institute'', Moscow. The typical nanodiamond powder sample image obtained by transmission electron microscopy at an accelerating voltage of 300 kV is shown in Fig. 2. The image clearly

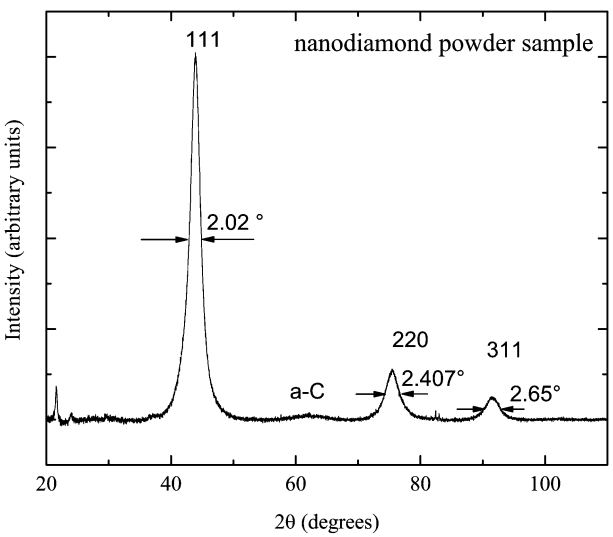

Fig. 1 X-ray diffraction pattern of the nanodiamond powder sample.

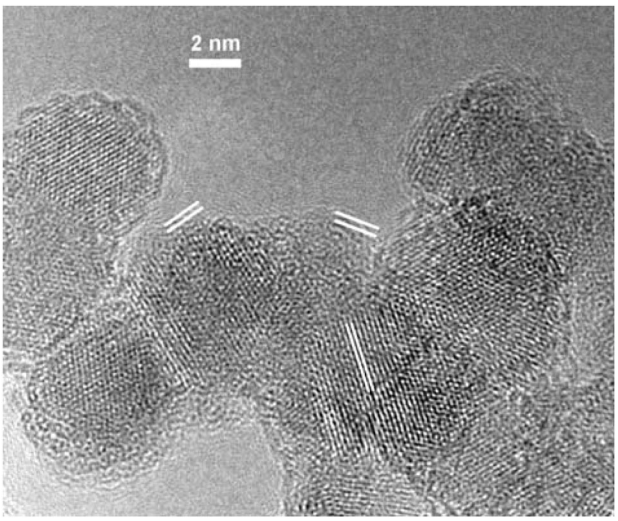

Fig. 2 The TEM image of the nanodiamond powder sample. The interplanar distance between the core planes is 2.1 Å and between the shell layers is 3.6–3.7 Å (both are highlighted by white lines).

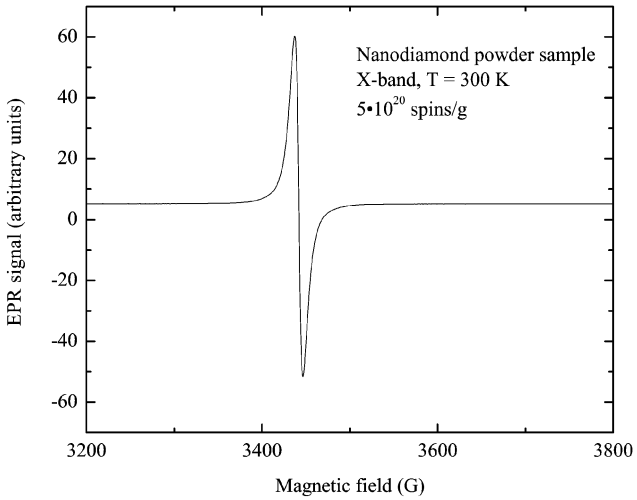

Fig. 3 cw EPR X-band spectrum of the nanodiamond powder sample measured at room temperature.

demonstrates the crystal structure of the diamond core covered by the shell of two–three amorphous carbon layers for every particle. The measured interplanar distance of the crystal core planes is 2.1 Å which corresponds to a diamond structure[1] (interplanar distance 2.06 Å in a diamond). The measured interplanar distances of the shell layers are close to 3.6–3.7 Å, which are typical for amorphous carbon onion layers.[30] Analysis of particle size distributions was performed using ImageJ software on a few TEM images and the following average diameter is $d = 6.7 \pm 1.7$ nm. The average shape of the nanodiamond particles is close to spherical (obtained circularity factor of 0.98 ± 0.09). The simulations of the corresponding X-ray diffraction pattern for the obtained nanodiamond size distributions with an average shell thickness of 0.9 ± 0.3 nm agree with the widths of the peaks from the measured XRD pattern.

EPR measurements

EPR experiments were carried out on a Bruker Elexsys E680 spectrometer at 9.7 and 94 GHz. The room temperature cw EPR spectrum consists of a single Lorentzian line with $g = 2.0044$ and HWHM = 0.85 mT (Fig. 3). Usually the similar lineshape and linewidth of the EPR signal correspond to the free radical-type center of the purified detonation nanodiamonds located in the diamond shell or on the surface.[1] Contribution of another type of paramagnetic center was detected using W-band echo-detected EPR, although its intensity did not exceed 10% of the total concentration, thus it was omitted during interpretation of the results. The signal of the N^0 centers was not observed. The only noticeable difference between the X and W-band EPR spectra was a twofold increase in linewidth.

The concentration of the paramagnetic centers in the nanodiamond sample is 5×10^{20} spin per g as was determined in the X-band at room temperature using a $Cu^{2+}(DETC)_2$ sample with a known number of spins.

Spin–spin (T_2^e) and spin–lattice (T_1^e) relaxation times of the paramagnetic centers were measured at the W-band using Hahn echo decay and inversion-recovery pulse sequences, respectively. Relaxation curves were fitted by a single exponential function. The relaxation measurements were performed in the range of temperatures from 300 down to 8 K. Spin–lattice relaxation time T_1^e slowly increases from 20 to 60 μs with a decrease in temperature, whereas T_2^e remains almost constant at a value of 300 ns. The spin–lattice relaxation is almost independent at temperatures below 50 K, possibly due to a strong spin–spin interaction between near-surface paramagnetic centers (similar to the case of NV centers in the diamond[31]), therefore we expect T_1^e on the order of 100 microseconds at temperatures of the ^{3}He NMR experiments.

Adsorption isotherms

The sample in the NMR experiments was either preliminary covered by a number of nitrogen layers N or not covered ($N = 0$). The Brunauer–Emmett–Teller (BET) analysis[32] of the measured nitrogen adsorption isotherm at 77 K provides the specific surface area of the sample of $S = 342.8 \pm 3.9$ m^2 g^{-1}. The measured nitrogen adsorption isotherm allowed us to estimate the gas amount that is required to cover our nanodiamond powder with numbers of nitrogen layers close to one, two and four ($N = 0.96$; 2.15; 3.69).

Since all NMR experiments were performed with adsorbed ^{3}He accurate measurements of ^{3}He adsorption isotherms were done at a temperature of 4.2 K for all N values. The monolayer capacities of adsorbed ^{3}He on the sample surface were obtained by point A[33,34] technique. The found ^{3}He monolayer stp quantity for $N = 0$ is $V_{ads} = 24.1 \pm 1.6$ cm^3. Following the surface helium capacities,[35,36] the corresponding specific surface area of our sample is 342.0 ± 22.2 m^2 g^{-1} (^{3}He), which agrees well with the results of N_2 BET analysis.

With the assumption of non-porous spherical particles, the obtained specific surface area value provides the estimated average particle diameter:[28] $d = 6/(\rho S) = 5.51 \pm 0.21$ nm. This is in good agreement with XRD and TEM results.

Similar ^{3}He adsorption isotherms were measured for $N = 0.96$, 2.15 and 3.69 and the following ^{3}He monolayer capacities were obtained: 18.15 ± 0.19 cm^3, 14.40 ± 0.18 cm^3,

and 12.11 ± 0.14 cm^3, respectively. All obtained ^{3}He monolayer values were used in further NMR experiments to adjust the ^{3}He adsorbed monolayer coverage fraction and to determine the exact number of nitrogen layers.

Results

In this work NMR measurements were performed in adsorbed ^{3}He with the fraction x_3 = 0.45; 0.6; 0.8 and 1.0 of the monolayer on the nanodiamond surface with/without nitrogen coverage. Here x_3 denotes the amount of adsorbed ^{3}He in the fractions of monolayer capacity, and x_4 is defined in the same way for adsorbed ^{4}He. ^{3}He gas was injected into the cell at 4.2 K and then the ^{3}He adsorbed layer was annealed for about 1 h before NMR experiments.

All measured ^{3}He longitudinal magnetization recovery and transverse magnetization decay curves in this work are well described by a single exponential function. In the case of the sample not preplated with N_2 (N = 0) the relaxation rate is quite fast; T_1 is on the order of milliseconds, which is unusually short compared with the adsorbed ^{3}He spin–lattice relaxation on various diamagnetic samples.[37–39]

A set of temperature dependences of the ^{3}He longitudinal magnetization recovery times T_1 were measured for various ^{3}He adsorbed layer coverages of the sample with and without nitrogen preplate. Typical measured T_1^{-1} temperature dependences are presented in Fig. 4. All measured temperature dependences of T_1 and T_2 for various N and x_3 are presented in a log scale in the ESI.† The obtained temperature dependences have a parabolic shape *versus* inverse temperature. For convenience $T_1^{-1,\max}$ and $T_{\max}$ will denote the maximum spin–lattice relaxation rate and the corresponding temperature in the mentioned dependences. $T_{\max}$ decreases as the ^{3}He coverage fraction x_3 increases (Fig. 5). Especially, $T_{\max}$ shifts at complete ^{3}He monolayer surface coverages x_3 = 1.0.

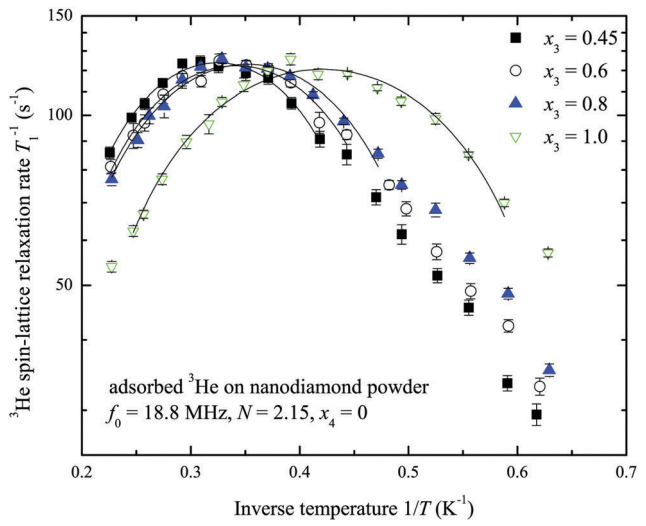

Fig. 4 Temperature dependences of ^{3}He spin–lattice relaxation rates T_1^{-1} at x_3 = 0.45, 0.6, 0.8 and 1.0 monolayer coverage of the nanodiamond powder sample preplated with nitrogen layers (N = 2.15, x_4 = 0). Solid lines represent fits by the parabolic function.

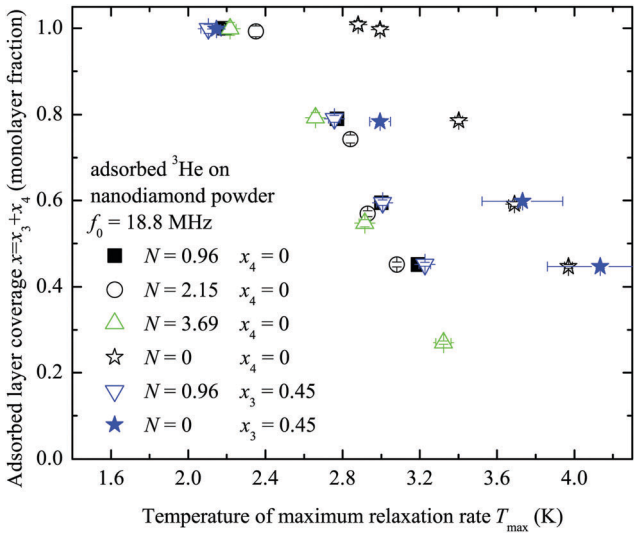

Fig. 5 The relation between the temperature of the ^{3}He spin–lattice relaxation maximum rate $T_1^{-1,\max}$ (Fig. 4) and the adsorbed ^{3}He coverage fraction x for performed experiments of adsorbed ^{3}He on the nanodiamond powder sample with the number of preplated nitrogen layers N = 0; 0.96; 2.15; 3.69.

The maximum values $T_1^{-1,\max}$ of the ^{3}He spin–lattice relaxation rate are slower for the case of the sample preliminarily covered by nitrogen layers. The obtained relation between $T_1^{-1,\max}$ and the number of nitrogen layers on the sample surface is displayed in Fig. 6 for various x_3 values. Clearly, the ^{3}He relaxation rate strongly depends on the number of nitrogen layers and rapidly decreases with N. $T_1^{-1,\max}$ is almost independent of x_3 except when N = 0.

Similar experiments were performed with a partial substitution of adsorbed ^{3}He with ^{4}He atoms for N = 0 and N = 0.96. The

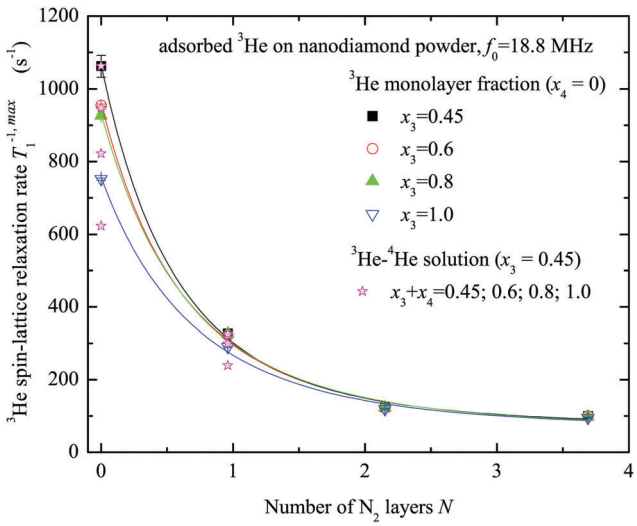

Fig. 6 Dependence of the ^{3}He spin–lattice relaxation rates $T_1^{-1,\max}$ at x_3 = 0.45, 0.6, 0.8 and 1.0 monolayer coverage of the nanodiamond powder sample on the number of preplated nitrogen layers N (x_4 = 0). Results of ^{3}He–^{4}He experiments are shown as supplementary data (x_3 = 0.45) (ESI†). Solid lines represent the fits by the relaxation model (see Appendix) and the following d_0 values are obtained: 0.43 ± 0.06; 0.49 ± 0.08; 0.54 ± 0.08; 0.61 ± 0.10 nm for x_3 = 0.45; 0.6; 0.8; 1.0, correspondingly.

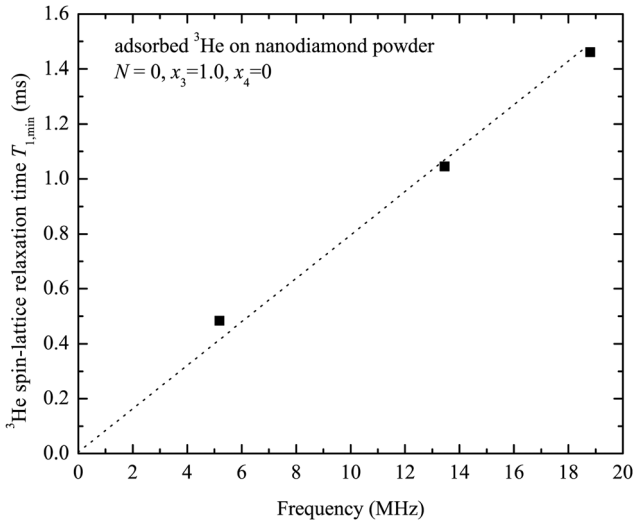

Fig. 7 The frequency dependence of the complete monolayer (x_3 = 1.0, x_4 = 0) ^{3}He spin–lattice relaxation times $T_{1,min}$ (N = 0) on the nanodiamond powder sample. The dashed line represents the $T_1 \propto \omega$ guideline.

x_3 = 0.45 amount of ^{3}He was adsorbed on the sample surface and then we increased the adsorbed layer density with x_4 amounts of ^{4}He to obtain similar layer coverages $x = x_3 + x_4$ = 0.45; 0.6; 0.8; 1.0 as before. In these experiments the observed T_{max} ($x = x_3 + x_4$) values are the same (within experimental error) as those in pure ^{3}He experiments (x_4 = 0) with N = 0.96 (see Fig. 5 and 6), but the ^{3}He spin–lattice relaxation rate slows down within 5–20% in general compared to that for x_4 = 0. The observed T_{max} *vs.* x for N = 0 does not coincide with the one of pure ^{3}He experiments (Fig. 5).

Fig. 7 shows the measured frequency dependence of the ^{3}He spin–lattice relaxation time $T_{1,min}$ (corresponds to $T_1^{-1,max}$) for a complete ^{3}He monolayer (x_3 = 1.0, N = 0). The observed ^{3}He relaxation time linearly increases with the Larmor frequency ω.

The temperature dependences of spin–spin relaxation times T_2 of the adsorbed ^{3}He were also measured at various x_3 coverages (x_4 = 0, see ESI†). The typical T_2 temperature dependences are presented in Fig. 8 for the sample with nitrogen preplate N = 0.96. T_2 values decrease as the temperature T decreases and a small T_2 deviation is observed between x_3 coverages.

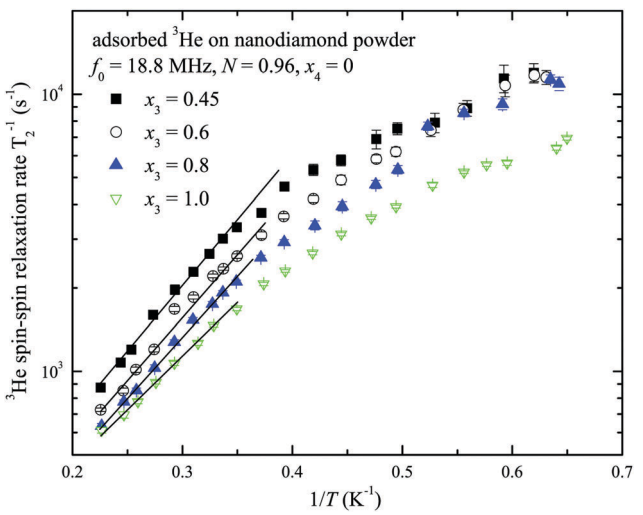

Fig. 8 The temperature dependences of ^{3}He spin–spin relaxation times T_2 at x_3 = 0.45, 0.6, 0.8 and 1.0 monolayer coverage of the nanodiamond powder sample preplated with one nitrogen layer nanodiamond powder sample (N = 0.96, x_4 = 0). The solid lines represent the fits by eqn (3) and (4) (see Discussion).

Discussion

The observed extremes in temperature dependence of ^{3}He relaxation rates $T_1^{-1}(T)$ provide information on the correlation times τ of fluctuating magnetic fields causing relaxation as well as values of the fluctuating magnetic fields themselves. Matsushita *et al.*[23] registered T_1 minima in ^{3}He adsorbed in the nanochannels of porous silicate powder and reported on the decrease of T_{max} temperature with an x_3 increase. Their findings were similar to our results, however they did not consider the influence of possible paramagnetic impurities and attribute this effect solely to ^{3}He movements in flat 2D films[13] as was done earlier by Cowan and Crane for boron nitride samples.[40,41]

Firstly, we shall check whether intrinsic dipole–dipole interactions in the ^{3}He film could be responsible for the observed relaxation. At the maximum relaxation rate when $\omega\tau \approx 1$ according to a simple three dimensional picture for the BPP (Bloembergen–Purcell–Pound) model one has:

$$T_{1,min} \approx \omega(\gamma_I^2\langle B_{loc}^2\rangle)^{-1}, \quad (1)$$

where $\langle B_{loc}^2\rangle$ is the mean square of the fluctuating magnetic field experienced by ^{3}He spins and $\gamma_I = 2\pi \times 32.43$ MHz T^{-1} is the ^{3}He gyromagnetic ratio. Note that at the condition of $\omega\tau$ = 1 a similar relation to eqn (1) can be easily derived for the case of nuclear spin relaxation through paramagnetic centers up to a constant factor (for instance, in the case of fixed spins using eqn (6) and (7) we obtain a factor of 0.08). This suggests that the $T_{1,min}$ proportionality to the Larmor frequency is not the only attribute of the ^{3}He–^{3}He dipole–dipole relaxation mechanism[12] but can also be observed when the relaxation of the nuclear spin occurs through paramagnetic centers. Indeed, the minimum of the relaxation time $T_{1,min}$ is proportional to the frequency for our data at which the $\omega\tau$ = 1 condition is satisfied (Fig. 7). Note that according to the relaxation theory of ^{3}He due to ^{3}He–^{3}He dipole–dipole interactions in the 2D layer[12] $T_{1,min}x_3^3 \propto \omega$, whereas we found an almost independent $T_{1,min}$ on x_3.

Assuming that ^{3}He–^{3}He dipole–dipole interactions are responsible for relaxation the estimates of a standard deviation of a fluctuating magnetic field (eqn (1)) lie within 1–3 mT depending on the number of nitrogen layers on the ND surface. These estimates of fluctuating magnetic field are too high compared to ones previously reported for a ^{3}He ensemble (0.1 mT as found for x_3 = 0.32 at 3.26 MHz and 1.8 K by Lusher *et al.*[22]). On the other hand the temperatures T_{max} depend on ^{3}He coverage x_3 (Fig. 5), but

$T_1^{-1,\max}$ remains the same for a fixed N (Fig. 4). All these facts additionally point out that observed ^{3}He relaxation is not governed by ^{3}He–^{3}He dipole–dipole coupling but involves an external magnetic reservoir.

The temperatures $T_{\max}$ for a given x_3 in pure ^{3}He experiments do not vary with the number of nitrogen layers when $N \geq 1$ (Fig. 5). This means that $T_{\max}$ strongly depends on the surface diffusive motion which is linked with the ^{3}He total density x_3. The observed $T_{\max}(x)$ for $N = 0$ differs from $N \geq 1$ because ^{3}He motion on a non-preplated surface is distinct. The $T_{\max}(x)$ and $T_1^{-1,\max}(N)$ relations in ^{3}He–^{4}He experiments ($N \geq 1$) are similar to the ones of pure ^{3}He because ^{3}He atom mobility does not change as ^{4}He replaces ^{3}He (Fig. 5 and 6).

The decrease of $T_1^{-1,\max}$ with N (see Fig. 6) unambiguously indicates that relaxation depends on the distance from the adsorbed ^{3}He to the nanodiamond surface. The data for ^{3}He–^{4}He presented on the same figure demonstrate similar relaxation rates and reflect the same tendency. Possibly the relaxation process involves paramagnetic centers, the concentrations of which are about 5×10^{20} spin per g. The ^{3}He amounts in our experiments do not exceed $n_3 = 6 \times 10^{20}$ spins at most, whereas the number of paramagnetic centers is about $n_{PC} = 9 \times 10^{19}$ (according to the sample weight), so for all experimental conditions we have:

$$n_{PC}\gamma_S(T_1^e)^{-1} \gg n_3\gamma_I T_1^{-1,\max}. \quad (2)$$

This means that the paramagnetic centers reservoir is indeed capable of absorbing magnetic energy from the nuclei system.

The condition of relaxation rate maximum ($\omega\tau \approx 1$) gives estimates for $\tau \approx 8.5$ ns. This time scale is much shorter than the measured spin–lattice relaxation time of paramagnetic centers T_1^e in nanodiamonds at low temperatures ($\approx$300 μs), and is also shorter than the spin–spin relaxation time $T_2^e \approx 300$ ns. Obviously T_2^e is not a correlation time for ^{3}He nuclear relaxation because the correlation time has an activation nature at low temperature and depends on the amount of ^{3}He (see Fig. 8). The found correlation time is likely associated with the ^{3}He surface diffusion that has either an activation nature (Arrhenius-like) or quantum tunneling between adsorption sites. Thermal motional averaging is indicated by the measured ^{3}He free induction decay characteristic time T_2^* that is proportional to the temperature: $T_2^*[\mu s] = (85.9 \pm 1.7)\cdot T$ [K] in the 1.5–4.2 K range for $x_3 = 1.0$. Let us assume that correlation time is the time needed for a ^{3}He atom to diffuse from one paramagnetic center to another near the surface. Assuming $D \sim 10^{-7}$ cm^2 s^{-1} in the ^{3}He layer at low temperatures[42] and that the paramagnetic centers are located in the nanodiamond shell near the surface with a mean distance between them $d \approx 0.9$ nm (corresponds to the surface mean density in assumption of surface paramagnetic centers), we get $\tau = d^2/4D \sim 20$ ns which agrees with observed correlation times.

Thus, the relaxation occurs through surface diffusional motions of nuclear spins in the magnetic fields mainly created by paramagnetic centers. This allows one to find the average distance from paramagnetic centers to the surface by applying the relaxation model described in the Appendix. This model implies the relaxation of nuclear longitudinal magnetization through paramagnetic centers distributed near the surface and intrinsic dipolar relaxation in the ^{3}He film. The observable longitudinal magnetization recovery is a single exponential because of the ^{3}He surface diffusive motion. This is different from the reported multiexponential processes of magnetization relaxation of immobile ^{1}H and ^{19}F nuclei spins at the surface of nanodiamonds[7,43] or ^{13}C inside the nanodiamonds.[44] A more detailed theory of nuclear magnetic relaxation in 2D fluids due to ^{3}He–^{3}He and ^{3}He–paramagnetic center dipole–dipole interactions mediated by 2D motions is given by Satoh and Sugawara.[45] Although we consider in details in Appendix the case of fixed nuclei and paramagnetic centers it gives the same distance dependence for longitudinal relaxation rates on the distance a from the ^{3}He film to paramagnetic centers ($T_1^{-1} \propto a^{-4}$ in 2D case). Another possible mechanism of nuclear magnetic relaxation in that system is considered by Kondo *et al.*[46] and Lusher *et al.*[47] The authors of these works suggested that relaxation occurs due to fast spin exchange between the bulk (liquid or gas) and solid adsorbed layer where strong local magnetic fields B_{loc} are almost constant during the ^{3}He short stay in the adsorbed layer. In that case the correlation time stands for the inversed exchange frequency and the longitudinal relaxation rate is proportional to $\langle B_{loc}{}^2\rangle$ averaged over the surface. Therefore the longitudinal relaxation rate has the same distance dependence as in our model. Thus, independent of the details of relaxation mechanisms, the distance dependence for longitudinal relaxation is similar and that allows us to determine distance from the fits.

The fits of experimental data by eqn (9) and (12) (see Fig. 6) yield the average distance from paramagnetic centers to the nanodiamond surface $d_0 = 0.5 \pm 0.1$ nm. Here it was assumed that the distance between adsorbed N_2 layers $d_{N_2-N_2}$ is the same between each adjacent atomic N_2 layer and is equal to 3.1 Å, as determined in numerous studies of adsorbed N_2 structure at low temperatures (see for instance the work of Golebiowska *et al.*[48]). The distance between the first adsorbed layer and the nanodiamond surface d_1 was also taken to be equal to 3.1 Å for the sake of simplicity (close to estimates for ^{3}He on Grafoil reported by Joly *et al.*[49]). The diameter of the nanoparticle was fixed to $d = 5.51$ nm, but we found that the fitting parameters are almost independent of d if the latter is chosen in the range 3–10 nm. In this fit we use an N-independent relaxation rate $T_1^{-1,dd}$ which is attributed to the self ^{3}He–^{3}He dipole–dipole relaxation in the adsorbed ^{3}He layer (eqn (12)) and has been under study for a long time (see all references from here regarding ^{3}He experiments). The obtained $T_1^{dd} \approx 14 \pm 2$ ms from the fits is short compared to those usually observed in ^{3}He adsorbed on various amorphous non-magnetic materials such as aerogels and Vycor (0.1–1 seconds)[36,37] and crystal powders,[40] but similar to those observed in FSM (Folded Sheet Mesoporous materials).[23]

The application of eqn (7) and (9) with $d_0 = 0.5$ nm provides a satisfactory agreement of the model relaxation time $T_1^{PC}(N = 0) = 4.1$ ms (the case of fixed spins is applied for the sake of simplicity) with the experimental $T_1 \approx 1$ ms at a frequency of 18.8 MHz. In this estimate we assumed the average number of paramagnetic centers in each particle $N_{PC} = 139$ which

corresponds to that defined above the mean diameter of nanoparticles and the total number of paramagnetic centers n_{PC}. Note that the measured value of $T_1 \approx 1$ ms can be obtained within this model for $d_0 = 0.3$ nm which is also close to the determined above average d_0.

Possibly, the applied technique for distance measurement can be implemented for the determination of types of paramagnetic centers and their location in nanodiamonds by selective ^{3}He relaxation measurements using the fact that paramagnetic centers of a different nature have different dynamic parameters. As the interaction between ^{3}He and paramagnetic centers is mutual, a similar idea can be applied for the same purpose by means of selective T_1^e measurements with a variable thickness of solid layers of nitrogen (or noble gas atoms) on the nanodiamond surface isolating nuclear and paramagnetic center systems. The measured single line of the EPR spectra in our sample is accumulated for a relatively broad nanodiamond size distribution. It is known that for particles smaller than 80 nm the concentration of paramagnetic centers strongly depends on the particle size.[50] In addition, the number of paramagnetic spins is very high and the paramagnetic spin system is strongly coupled. Therefore it makes it impossible to distinguish different types of paramagnetic centers by means of EPR and ^{3}He NMR. Such a type of experiment can be carried out in nanodiamonds with a lower concentration of paramagnetic centers and a narrow size distribution, which is not the case for our sample.

Temperature dependences of ^{3}He transverse relaxation clearly show an exponential decrease of relaxation times T_2 with inverse temperature $1/T$ (Fig. 8). The observed relaxation time values and temperature behaviour are similar to that of reported 2D films of ^{3}He.[23,45,46] Additionally we found a weaker dependence of T_2 than of T_1 on the number of nitrogen layers (see ESI†). This points out that the influence of intrinsic dipole–dipole relaxation in the ^{3}He film on transverse ^{3}He relaxation is stronger (eqn (13)). Moreover we note that relaxation time T_2 in 2D is always much shorter than T_1 in dipolar coupled systems (nuclear–nuclear and/or nuclear–electron) due to peculiarities of dipolar correlation functions in reduced dimensions.[13,45]

At low temperatures (below 2 K) T_2 is independent on temperature and indicates crossover from thermally activated motion to quantum tunneling as is known, for instance, from studies of ^{3}He in Vycor.[36] A commonly used rule-of-thumb for motionally narrowed 3D systems reads:

$$T_2^{-1} = \tau M_2, \quad (3)$$

where τ is the correlation time of motion, and M_2 is the second moment of the rigid lattice NMR adsorption line. The activation energy for atomic motion E_a is linked with correlation time of thermal motions through the Arrhenius law:

$$\tau^{-1} \propto \exp(-E_a/kT). \quad (4)$$

The fits of the high temperature part of T_2 temperature dependences by eqn (4) yield activation energies E_a. The obtained activation energy values lie in the range from 9 to 14 K depending on x_3. A decrease of activation energy E_a with x_3 is observed. This behaviour is consistent with the increase of T_{max} for T_1^{-1} with x_3. The obtained absolute values of E_a and $T_{max}(x)$ dependences are similar to those previously reported by Matsushita *et al.*,[23] but opposite to ones obtained for ^{3}He in hexagonal boron nitride.[41]

Conclusions

We have performed NMR measurements of adsorbed ^{3}He in nanodiamond powders in the 1.5–4.2 K temperature range. The observed maxima in T_1^{-1} temperature dependences are clearly interpreted by the suggested relaxation model *via* paramagnetic impurities. The ^{3}He relaxation rates strongly depend on the distance from the ^{3}He layer to the nanodiamond surface and are governed by fluctuating fields experienced by diffusing nuclear spins. These fields are created by paramagnetic centers and are modulated by ^{3}He thermal and quantum tunneling surface motions. The suggested relaxation model allows the quantitative determination of the location of near-surface paramagnet centers in the nanodiamond sample with angstrom precision. The same experimental technique and relaxation model could prospectively be used to distinguish the core paramagnetic centers in nanodiamond samples with a reduced amount of surface paramagnetic centers. The distance dependence of the ^{3}He relaxation rate ($T_1^{-1} \propto a^{-4}$ for 2D case) is not sensitive to the details of the system (2D solid, 2D fluid or gas–solid with fast exchange). The observed large difference between T_1 and T_2 is explained by the difference in dominating mechanisms responsible for longitudinal and transverse relaxation: ^{3}He–paramagnetic centers and ^{3}He–^{3}He dipolar interactions, correspondingly. The determined average distance from the paramagnetic centers to the nanodiamond surface of 0.5 ± 0.1 nm shows that these paramagnetic centers are located in the nanodiamond shell. This is consistent with the well-known information on nanodiamond structures and the EPR measurements. The proposed technique to probe the location of the paramagnetic centers that uses adsorbed ^{3}He and N_2 layers can be applied to studies of various nanosized samples with paramagnetic impurities. The demonstrated method can also be performed with adsorbed layers of noble gases instead of nitrogen.

Author contributions statement

V. K., K. S. and A. Kl. designed and performed the NMR experiments and contributed to the analysis of experimental results and to the discussion. G. D., A. S. and E. A. also conducted NMR and gas adsorption experiments, and participated in sample preparation. T. S. contributed to low-temperature experimental equipment assembly. B. Y. and S. O. performed EPR experiments and contributed to the discussion, A. K. performed XRD measurements and M. P. performed TEM imaging. M. T. defined the original research objectives and contributed to the experiment design. All authors contributed to manuscript writing.

Conflicts of interest

There are no conflicts of interest to declare.

Appendix: relaxation model

For simplicity we shall consider an ideal spherical nanoparticle in which the paramagnetic centers are distributed in the surface layer on the same distance from the surface d_0 (Fig. 9). According to different physical models of ^{3}He longitudinal relaxation through paramagnetic centers described in the Discussion section, we can write:

$$\Gamma_1 \propto \langle B_{\mathrm{loc}}{}^2 \rangle, \tag{5}$$

where Γ_1 is the nuclear longitudinal relaxation rate. Then taking into account that $B_{\mathrm{loc}} \propto r^{-3}$, where r is the distance between the nucleus and paramagnetic center, we can write the nuclear relaxation rate on the nanoparticle surface through a single paramagnetic center:

$$\Gamma_1 = C\left\langle \frac{1}{r^6} \right\rangle_{\mathrm{surf}}, \tag{6}$$

where $\langle\rangle_{\mathrm{surf}}$ denotes an average taken on a sphere of radius $(R + a)$.

Note that for the fixed spins:[51]

$$C \approx \frac{2}{5}\gamma_{\mathrm{S}}{}^2\gamma_{\mathrm{I}}{}^2\hbar^2 S(S+1)\frac{\tau}{1+\omega^2\tau^2}, \tag{7}$$

where γ_{S} and γ_{I} are gyromagnetic ratios of the paramagnetic centers and nuclei, correspondingly; $\hbar$ is the Plank constant, S is the electronic spin, τ is the correlation time of fluctuating magnetic fields causing relaxation, and ω is the Larmor frequency.

Let us assume that the paramagnetic center is located at a distance d_0 from the surface, ^{3}He is at a distance d_1 from the surface, R_0 is the radius of nanoparticle and $R = R_0 - d_0$ and $a = d_0 + d_1$. Then one can get:

$$\Gamma_1 = \frac{C}{2\pi}\int_0^{\pi} \frac{\sin\varphi}{(R^2 + (R+a)^2 - 2R(R+a)\cos\varphi)^3}\mathrm{d}\varphi, \tag{8}$$

where the average is taken on the sphere of radius $R_0 + d_1$.

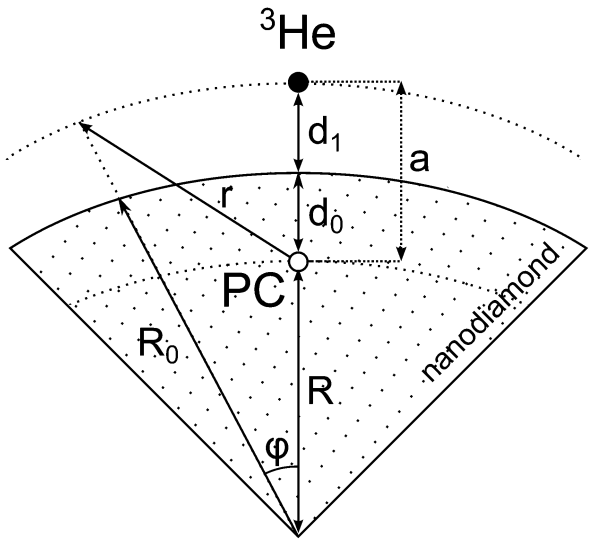

Fig. 9 An illustration of the developed relaxation model of ^{3}He adsorbed on the nanodiamond surface.

Finally, assuming no correlations between magnetic fields created by different paramagnetic centers and taking the above integral, we found a total relaxation rate due to all paramagnetic centers in the nanoparticle:

$$\frac{1}{T_1^{\mathrm{PC}}} = N_{\mathrm{PC}}\Gamma_1 = \frac{N_{\mathrm{PC}}C(\xi^2 + 2\xi + 2)}{R^6\xi^4(\xi+2)^4}, \tag{9}$$

where

$$\xi = \frac{d_0 + d_1}{R_0 - d_0}, \tag{10}$$

N_{PC} is the number of paramagnetic centers in each nanoparticle.

The result given by eqn (9) can be applied to a nanoparticle preplated with nitrogen layers. For that case d_1 should be substituted in eqn (10) by:

$$d_2 = d_1 + Nd_{\mathrm{N_2\text{–}N_2}}, \tag{11}$$

where N is the number of nitrogen monolayers and $d_{\mathrm{N_2\text{–}N_2}}$ is the distance between adjacent monolayers.

Note that in the case of large nanoparticles ($\xi \ll 1$, in another words $a \ll R$) one has $T_1^{-1,\mathrm{PC}} \propto a^{-4}$ dependence of relaxation rate on the distance from paramagnetic centers to the ^{3}He layer as it follows from eqn (9).

In addition to this relaxation mechanism described above one has to take into account intrinsic dipolar relaxation in ^{3}He films (T_1^{dd}). Thus, the observable longitudinal relaxation time of adsorbed ^{3}He can be described by the following equation:

$$\frac{1}{T_1} = \frac{1}{T_1^{\mathrm{PC}}} + \frac{1}{T_1^{\mathrm{dd}}}. \tag{12}$$

And similarly,

$$\frac{1}{T_2} = \frac{1}{T_2^{\mathrm{PC}}} + \frac{1}{T_2^{\mathrm{dd}}}. \tag{13}$$

Acknowledgements

This work was financially supported by the Russian Science Foundation (grant RSF 16-12-10359). The experimental part of this work was partially done on equipment of the RC of Probe and EM (Kurchatov Complex of NBICS-Technologies, NRC "Kurchatov Institute").

References

1 O. A. Shenderova, *Detonation nanodiamonds: science and applications*, Pan Stanford Publishing, 2014.
2 S. Koizumi, C. Nebel and M. Nesladek, *Physics and applications of CVD diamond*, John Wiley & Sons, 2008.
3 B. Yavkin, G. Mamin and S. Orlinskii, *J. Magn. Reson.*, 2016, **262**, 15.
4 B. V. Yavkin, V. A. Soltamov, R. A. Babunts, A. N. Anisimov, P. G. Baranov, F. M. Shakhov, S. V. Kidalov, A. Y. Vul', G. V. Mamin and S. B. Orlinskii, *Appl. Magn. Reson.*, 2014, **45**, 1035.
5 S. B. Orlinskii, R. S. Bogomolov, A. M. Kiyamova, B. V. Yavkin, G. M. Mamin, S. Turner, G. Van Tendeloo,

A. A. Shiryaev, I. I. Vlasov and O. Shenderova, *Nanosci. Nanotechnol. Lett.*, 2011, **3**, 63.
6 A. M. Panich, A. Altman, A. I. Shames, V. Y. Osipov, A. E. Aleksenskiy and A. Y. Vul, *J. Phys. D: Appl. Phys.*, 2011, **44**, 125303.
7 A. M. Panich, *Crit. Rev. Solid State Mater. Sci.*, 2012, **37**, 276.
8 T. Staudacher, F. Shi, S. Pezzagna, J. Meijer, J. Du, C. A. Meriles, F. Reinhard and J. Wrachtrup, *Science*, 2013, **339**, 561.
9 N. Aslam, M. Pfender, P. Neumann, R. Reuter, A. Zappe, F. Fávaro de Oliveira, A. Denisenko, H. Sumiya, S. Onoda, J. Isoya and J. Wrachtrup, *Science*, 2017, DOI: 10.1126/science.aam8697.
10 F. Fávaro de Oliveira, S. A. Momenzadeh, D. Antonov, J. Scharpf, C. Osterkamp, B. Naydenov, F. Jelezko, A. Denisenko and J. Wrachtrup, *Nano Lett.*, 2016, **16**, 2228.
11 T. Rendler, J. Neburkova, O. Zemek, J. Kotek, A. Zappe, Z. Chu, P. Cigler and J. Wrachtrup, *Nat. Commun.*, 2017, **8**, 14701.
12 B. Cowan, L. A. El-Nasr, M. Fardis and A. Hussain, *Phys. Rev. Lett.*, 1987, **58**, 2308.
13 B. P. Cowan, *J. Phys. C: Solid State Phys.*, 1980, **13**, 4575.
14 H. Godfrin and H.-J. Lauter, *Prog. Low Temp. Phys.*, 1995, **14**, 213.
15 N. S. Sullivan, *J. Low Temp. Phys.*, 1976, **22**, 313.
16 L. J. Friedman, T. J. Gramila and R. C. Richardson, *J. Low Temp. Phys.*, 1984, **55**, 83.
17 D. R. Swanson, D. Candela and D. O. Edwards, *J. Low Temp. Phys.*, 1988, **72**, 213.
18 A. Schuhl, S. Maegawa, M. W. Meisel and M. Chapellier, *Phys. Rev. Lett.*, 1985, **54**, 1952.
19 S. Saito, *Phys. Rev. Lett.*, 1976, **36**, 975.
20 A. Egorov, F. Aukhadeev, M. Tagirov and M. Teplov, *JETP Lett.*, 1984, **39**, 480.
21 A. V. Egorov, D. S. Irisov, A. V. Klochkov, A. V. Savinkov, K. R. Safiullin, M. S. Tagirov, D. A. Tayurskii and A. N. Yudin, *JETP Lett.*, 2007, **86**, 416.
22 C. P. Lusher, J. Nyéki, D. Shvarts, B. P. Cowan, J. Saunders and D. E. W. Vaughan, *J. Low Temp. Phys.*, 2004, **134**, 619.
23 T. Matsushita, R. Kawai, A. Kuze, M. Hieda and N. Wada, *J. Low Temp. Phys.*, 2014, **175**, 407.
24 E. Alakshin, R. Gazizulin, A. Klochkov, V. Kuzmin, A. Sabitova, T. Safin and M. Tagirov, *Magnetic Resonance in Solids*, 2013, **15**, 13104.
25 F. V. Keuls, T. Gramila, L. Friedmant and R. Richardson, *Phys. B*, 1990, **165**, 717.
26 M. Malkov, *Handbook on the Physicotechnical Fundaments of Deep Cooling [Spravochnik po fiziko-tehnicheskim osnovam glubokogo ohlazhdeniya]*, Gosenergoizdat, Moscow, 1963.
27 Z. Qiao, J. Li, N. Zhao, C. Shi and P. Nash, *Scr. Mater.*, 2006, **54**, 225.
28 V. Pichot, M. Comet, E. Fousson, C. Baras, A. Senger, F. L. Normand and D. Spitzer, *Diamond Relat. Mater.*, 2008, **17**, 13.
29 A. K. Arora, T. Ravindran, G. Reddy, A. K. Sikder and D. Misra, *Diamond Relat. Mater.*, 2001, **10**, 1477.
30 O. O. Mykhaylyk, Y. M. Solonin, D. N. Batchelder and R. Brydson, *J. Appl. Phys.*, 2005, **97**, 074302.
31 A. Jarmola, V. M. Acosta, K. Jensen, S. Chemerisov and D. Budker, *Phys. Rev. Lett.*, 2012, **108**, 197601.
32 S. Brunauer, P. H. Emmett and E. Teller, *J. Am. Chem. Soc.*, 1938, **60**, 309.
33 P. H. Emmett and S. Brunauer, *J. Am. Chem. Soc.*, 1937, **59**, 1553.
34 M. Bretz, J. G. Dash, D. C. Hickernell, E. O. McLean and O. E. Vilches, *Phys. Rev. A: At., Mol., Opt. Phys.*, 1973, **8**, 1589.
35 J. G. Daunt and E. Lerner, *J. Low Temp. Phys.*, 1972, **8**, 79.
36 J. G. Daunt and E. Lerner, *Monolayer and Submonolayer helium films*, Springer, 1973.
37 A. V. Klochkov, V. V. Kuz'min, K. R. Safiullin, M. S. Tagirov, D. A. Tayurskii and N. Mulders, *JETP Lett.*, 2008, **88**, 823.
38 D. J. Creswell, D. F. Brewer and A. L. Thomson, *Phys. Rev. Lett.*, 1972, **29**, 1144.
39 D. P. Grimmer and K. Luszczynski, *J. Low Temp. Phys.*, 1978, **30**, 153.
40 T. P. Crane and B. P. Cowan, *Phys. Rev. B: Condens. Matter Mater. Phys.*, 2000, **62**, 11359.
41 T. Crane and B. Cowan, *Phys. B*, 2000, **284–288**(Part 1), 230.
42 B. Cowan, M. Fardis, T. Crane and L. Abou-El-Nasr, *Phys. B*, 1990, **165-166**, 707.
43 A. M. Panich, H.-M. Vieth, A. I. Shames, N. Froumin, E. Osawa and A. Yao, *J. Phys. Chem. C*, 2010, **114**, 774.
44 A. M. Panich, N. A. Sergeev, A. I. Shames, V. Y. Osipov, J.-P. Boudou and S. D. Goren, *J. Phys.: Condens. Matter*, 2015, **27**, 072203.
45 K. Satoh and T. Sugawara, *J. Low Temp. Phys.*, 1980, **38**, 37.
46 Y. Kondo, T. Mizusaki, A. Hirai, Y. Hirayoshi and K. Eguchi, *J. Low Temp. Phys.*, 1989, **75**, 289.
47 C. P. Lusher, M. F. Secca and M. G. Richards, *J. Low Temp. Phys.*, 1988, **72**, 25.
48 M. Golebiowska, L. Firlej, B. Kuchta and R. Fabianski, *J. Chem. Phys.*, 2009, **130**, 204703.
49 F. Joly, C. Lhuillier and B. Brami, *Surf. Sci.*, 1992, **264**, 419.
50 B. Yavkin, G. Mamin, M. Gafurov and S. Orlinskii, *Magnetic Resonance in Solids*, 2015, **17**, 15101.
51 A. Abragam, *The principles of nuclear magnetism*, Oxford university press, 1961.